Brueckner-Goldstone Many-Body Theory for Dynamic Polarizabilities: Application to Ne†

C. Matsubara,* N. C. Dutta,* T. Ishihara, and T. P. Das*
Department of Physics, University of California, Riverside, California 92502

A many-body procedure applied earlier to helium is utilized here to study the response of a neon atom in its ground state to a time-dependent electric field. The theory of the method, omitted in the helium paper for reasons of brevity, is included here. Our results for the frequency-dependent polarizabilities $\alpha(\omega)$ lead to refractive indices $n(\omega)$, in excellent agreement with experiment. As a by-product of the calculation, we obtain [from the poles of $\alpha(\omega)$] excitation energies for $2p \rightarrow ns$ and $2p \rightarrow nd$ transitions in good agreement with experiment.

I. INTRODUCTION

There is considerable current interest in the response of atomic systems to time-dependent perturbing fields.[1-5] The main reason for this interest is that this response function provides information about the properties of excited states and of interacting atoms.[6-10] In an earlier communication,[4] we have reported briefly the results of our calculation of dynamic polarizability $\alpha(\omega)$ of helium $(1s^2; {}^1S)$ through an adaptation of the Brueckner-Goldstone (BG) many-body theory. The excitation energies and London constants between hydrogen-helium and helium-helium atoms derived from $\alpha(\omega)$ have also been reported.[6] The purpose of the present paper is to report the results of a many-body calculation of $\alpha(\omega)$ for neon atom $(1s^2 2s^2 2p^6; {}^1S)$ ground state. Also we take this opportunity to present the details of the theory for utilization of the BG procedure for time-dependent perturbation, which we had not been able to present in the earlier paper[4] due to lack of space.

The calculation of $\alpha(\omega)$ for neon is more interesting than helium since neon involves more shells and provides a more severe test of the applicability of the BG method and a richer analysis of many-body effects. Another reason for the present calculation is that earlier one-electron analysis of $\alpha(\omega)$ and excitation energies of neon[3] did not yield good agreement with experiment, the discrepancy being more significant than for helium.[3,4] It is of interest to see if the present method of calculation can bridge the gap between theory and experiment.

In Sec. II, we can describe the general formulation of the BG theory for time-dependent perturbations. In Sec. III, we discuss our results for $\alpha(\omega)$ and excitation energies, and compare them with experiment and earlier work.

II. THEORY

The total Hamiltonian $\mathcal{H}(t)$ for an atom in the presence of a time-dependent external perturbation $\mathcal{H}_2'(t)$ is

$$\mathcal{H}(t) = \mathcal{H}_0 + \mathcal{H}_1' + \mathcal{H}_2'(t) \quad , \tag{2.1}$$

$$\text{where} \quad \mathcal{H}_0 = \sum_{i=1}^{N} (T_i + V_i) \quad , \tag{2.2}$$

$$\text{and} \quad \mathcal{H}_1' = \sum_{i>j}^{N} \frac{1}{r_{ij}} - \sum_{i=1}^{N} V_i \quad . \tag{2.3}$$

We shall assume a harmonic perturbation of the form

$$\mathcal{H}_2'(t) = G_\omega(\vec{\mathbf{r}})\, e^{i\omega t} + \text{c.c.} \tag{2.4}$$

In Eq. (2.2), T_i is the sum of the kinetic energy and the nuclear Coulomb energy of the ith electron; $1/r_{ij}$ is the Coulomb interaction energy between the ith and jth electrons; and N is the total number of electrons in the atom. V_i is a single-particle potential which we can choose suitably to obtain good convergence in perturbation theory and to simplify the computational procedure. The analysis of a perturbation of the type (2.4) enables us to handle any general perturbation because the latter can be expanded as a Fourier series in ω.

The N-particle eigenfunction Φ_n of the zero-order Hamiltonian $\mathcal{H}_0$, satisfying

$$\mathcal{H}_0 \Phi_n = E_n \Phi_n \quad , \tag{2.5}$$

can be expressed as combinations of Slater determinants built out of the complete set of one-electron states φ_i generated by

$$(T + V)\, \varphi_i = \epsilon_i \varphi_i \quad . \tag{2.6}$$

In general, this complete set of states will consist of both bound and continuum states. The unperturbed ground-state function Φ_0 is given by an appropriate linear combination of Slater determinants built out of single-electron states belonging to the

N lowest one-electron energy levels. Following usual notations, Eqs. (2.2)–(2.4) can be rewritten in second quantized form as

$$\mathcal{H}_0 = \sum_p \epsilon_p \eta_p^\dagger \eta_p \quad , \tag{2.7}$$

$$\mathcal{H}_1' = \sum_{p,q,r,s}{}' \langle pq|\frac{1}{r_{12}}|rs\rangle \eta_p^\dagger \eta_q^\dagger \eta_s \eta_r - \sum_{p,q} \langle p|V|q\rangle \eta_p^\dagger \eta_q \quad , \tag{2.8}$$

$$\mathcal{H}_2'(t) = \sum_{p,q} [\langle p|G_\omega(\vec{r})|q\rangle e^{i\omega t} + \langle p|G_\omega^*(\vec{r})|q\rangle e^{-i\omega t}] \eta_p^\dagger \eta_q \quad , \tag{2.9}$$

where η and $\eta^\dagger$ are annihilation and creation operators, respectively. The prime on the summation in (2.8) indicates that only distinct terms obtained from a combination of the four indices have to be included. Proceeding to the interaction representation denoted by subscript I, operators in the problem take the form

$$O_I(t) = e^{i\mathcal{H}_0 t} O(t) e^{-i\mathcal{H}_0 t}$$

Thus, the net perturbation Hamiltonian $\mathcal{H}'(t) = \mathcal{H}_1' + \mathcal{H}_2'(t)$ transforms to

$$\mathcal{H}_I'(t) = e^{i\mathcal{H}_0 t} \mathcal{H}'(t) e^{-i\mathcal{H}_0 t} e^{-\alpha|t|}; \quad \alpha \to 0^+ \quad , \tag{2.10}$$

where the factor $e^{-\alpha|t|}$ is added to denote adiabatic perturbation.[11] The ground-state wave function $\Psi(t)$ corresponding to the total Hamiltonian $\mathcal{H}(t)$ is then given in the interaction representation by

$$\Psi(t) = U(t, -\infty)\Phi_0 \quad , \tag{2.11}$$

where

$$U(t, t_0) = \sum_{n=0}^{\infty} U_n(t, t_0) = \sum_{n=0}^{\infty} \frac{(-i)^n}{n!} \int_{t_0}^{t} dt_1 \int_{t_0}^{t} dt_2 \cdots \times \int_{t_0}^{t} dt_n T[\mathcal{H}_I'(t_1) \cdots \mathcal{H}_I'(t_n)] \, . \tag{2.12}$$

The operator $U(t, t_0)$ is unitary which implies that $\Psi(t)$ is normalized to unity.[12] Hence, the expectation value of an operator O is given by

$$\langle O \rangle = \langle \Psi(t)|O_I(t)|\Psi(t)\rangle = \langle U(t, -\infty)\Phi_0|O_I(t)|U(t, -\infty)\Phi_0\rangle = \langle U(\infty, -\infty)\Phi_0|U(\infty, t)O_I(t)U(t, -\infty)|\Phi_0\rangle \, . \tag{2.13}$$

Assuming that ω is small compared with the first excitation energy, we can write

$$\Psi(\infty) = U(\infty, -\infty)\Phi_0 = e^{i\beta}\Phi_0 \quad , \tag{2.14}$$

where β is a real constant. Equation (2.13) can be reduced to the form

$$\langle 0 \rangle = \frac{\langle \Phi_0|U(\infty, t)O_I(t)U(t, -\infty)|\Phi_0\rangle}{\langle \Phi_0|U(\infty, -\infty)|\Phi_0\rangle} = \sum_{n,n'} \langle \Phi_0|U_n(\infty, t)O_I(t)U_{n'}(t, -\infty)|\Phi_0\rangle_L \quad , \tag{2.15}$$

where the subscript L indicates that only linked terms[13] should be included in the summation.

As in the case of time-independent problems[14–18] the terms in the summation in Eq. (2.15) can be represented by Feynman-like diagrams. The diagrammatic notations for the vertices are the same as before [4,6,15–18] except that we need the notations in Fig. 1 for the vertices $\mathcal{H}_2'(t)$ and O. Due to the time dependence of $\mathcal{H}_2'(t)$, some modifications are necessary in the rules for the energy denominators in the diagrams. We are interested here only in linear response so that the vertex $\mathcal{H}_2'(t)$ occurs

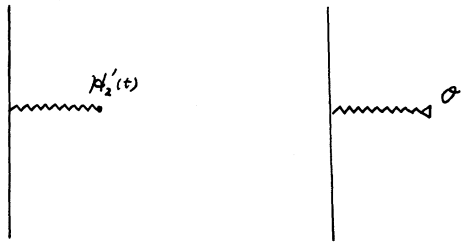

FIG. 1. Additional interaction vertices that enter into the polarizability calculations. The diagram on the left shows the vertex associated with the external time-dependent perturbation $\mathcal{H}_2'(t)$ while the diagram on the right describes an operator O, whose expectation value is being sought. [See Eqs. (2.13) and (2.15).] In the present investigation, the operator O has been taken to be the dipole moment operator Z.

FIG. 2. Diagrams describing the rules for energy denominators.

only once in each diagram. The modified rules are illustrated in Fig. 2. Thus, the parts of the diagrams between the $G_\omega e^{i\omega t}$ and O vertices have denominators $(E_0 - \mathcal{H}_0 \mp \omega)$ as indicated, with ω replaced by $-\omega$ in the case of $G^*_\omega e^{-i\omega t}$. All other denominators are the same as in the case of time-independent problems.[14-18] The generalization to nonlinear response involving more than one $\mathcal{H}_2'(t)$ vertex in the diagrams is straightforward.

For our present problem of frequency-dependent polarizabilities of atoms and molecules, we assume that the external perturbation originates from a plane-polarized electromagnetic wave in the Z direction. Thus, $\mathcal{H}_2'(t)$ is now given by

$$\mathcal{H}_2'(t) = \sum_{i=1}^{N} (E_0 Z_i e^{i\omega t} + \text{c.c.}) \quad . \tag{2.16}$$

Z_i being the Z coordinate of the ith electron, and $2E_0$ is the amplitude of the electromagnetic wave. O is now the dipole operator

$$O = \sum_{i=1}^{N} Z_i = Z \quad . \tag{2.17}$$

The polarizability $\alpha(\omega)$ is derived from the relation

$$\langle Z \rangle = -\alpha(\omega)(E_0 e^{i\omega t} + \text{c.c.}) \quad , \tag{2.18}$$

where $\langle Z \rangle = \sum_{n,n'} \langle \Phi_0 | U_n(\infty, t)$

$$\times Z_I(t) U_{n'}(t, -\infty) | \Phi_0 \rangle_L \tag{2.19}$$

The form of the right-hand side of (2.18) is a consequence of the linear response that we are presently interested in.

In listing the diagrams that we shall evaluate for $\alpha(\omega)$, a word about the nomenclature regarding orders in $\alpha(\omega)$ is helpful. Thus in writing

$$\alpha(\omega) = \sum_{n=0}^{\infty} \alpha_n(\omega); \quad \langle Z \rangle = \sum_{n=0}^{\infty} \langle Z \rangle_n \quad ; \tag{2.20}$$

the order n is determined by the number of $\mathcal{H}_1'$ vertices in the diagram, since the number of $\mathcal{H}_2'(t)$ and Z vertices are restricted to one each because of linear response.

Thus, $\langle Z \rangle_0$ is given by the sum of the diagrams shown in Fig. 3. The contribution to $\langle Z \rangle_0$ from these diagrams is

$$\langle Z \rangle_0 = E_0 \sum_{m,k} |\langle m | Z | k \rangle|^2 \left(\frac{e^{i\omega t}}{\epsilon_m - \epsilon_k - \omega} + \frac{e^{-i\omega t}}{\epsilon_m - \epsilon_k + \omega} + \frac{e^{i\omega t}}{\epsilon_m - \epsilon_k + \omega} + \frac{e^{-i\omega t}}{\epsilon_m - \epsilon_k - \omega} \right) , \tag{2.21}$$

thus giving $\alpha_0(\omega)$ from these diagrams as

$$\alpha_0(\omega) = -\sum_{m,k} |\langle m | Z | k \rangle|^2 \times [(\epsilon_m - \epsilon_k - \omega)^{-1} + (\epsilon_m - \epsilon_k + \omega)^{-1}] . \tag{2.22}$$

Here m represents the hole states and k represents the particle states. The summation over k implies a regular summation over bound excited states and an integration over the continuum states. The next order contribution $\alpha_1(\omega)$ arises from the diagrams which include one order of $\mathcal{H}_1'$ vertex. Four typical classes of diagrams that contribute to $\alpha_1(\omega)$ are presented in Fig. 4. The diagrams of class 4(a) and 4(b) could be interpreted as representing the first-order correction to the polarizability due to the self-consistent interaction between the perturbed hole states. In Fig. 4(b), the diagrams involving same hole states do not occur if we use the so called V^N-1 potential [4-6, 14-18] for the single-particle states. On the other hand, Figs. 4(c) and 4(d) are two-particle

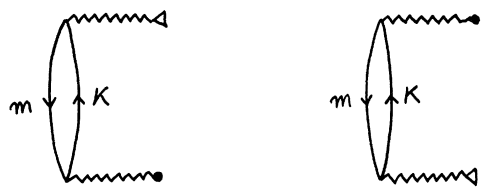

FIG. 3. Diagrams contributing to $\alpha_0(\omega)$.

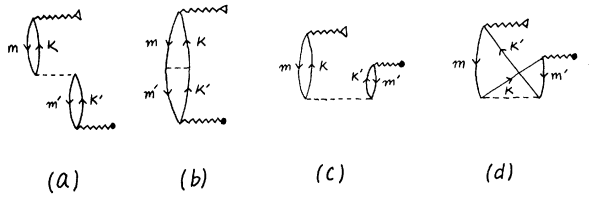

FIG. 4. Diagrams contributing to $\alpha_1(\omega)$. For each of the diagrams, all possible time ordering of interaction vertices should be included.

correlation diagrams, the latter class being the exchange counterpart of the former. For each of these classes one has to include all diagrams involving different time ordering and also include both $G_\omega e^{i\omega t}$ and $G_\omega^* e^{-i\omega t}$ vertices. Finally, it should be pointed out that in drawing these diagrams in Fig. 4 we have carried out the usual cancellation between the vertices associated with $1/r_{ij}$ and $-V_i$, as in our earlier work in time-independent problems.[15-18] The algebraic expressions for $\alpha_1(\omega)$ corresponding to these diagrams are given by

$$\alpha_1^{a}(\omega) = -\sum_{\substack{m,m'\\k,k'}} \langle m|\mathcal{Z}|k\rangle\langle km'|(r_{12})^{-1}|mk'\rangle$$

$$\times \langle k'|\mathcal{Z}|m'\rangle[(\epsilon_m - \epsilon_k - \omega)(\epsilon_{m'} - \epsilon_{k'} - \omega)]^{-1} + [(\epsilon_m - \epsilon_k + \omega)(\epsilon_{m'} - \epsilon_{k'} + \omega)]^{-1}\ ,$$

$$\alpha_1^{b}(\omega) = \sum_{\substack{m,m'\\k,k'}} \langle m|\mathcal{Z}|k\rangle\langle m'k|(r_{12})^{-1}|mk'\rangle$$

$$\times\langle k'|\mathcal{Z}|m'\rangle[(\epsilon_m - \epsilon_k - \omega)(\epsilon_{m'} - \epsilon_{k'} - \omega)]^{-1} + [(\epsilon_m - \epsilon_k + \omega)(\epsilon_{m'} - \epsilon_{k'} + \omega)]^{-1}\ , \qquad (2.24)$$

$$\alpha_1^{c}(\omega) = -\sum_{\substack{m,m'\\k,k'}} \langle m|\mathcal{Z}|k\rangle\langle m'|\mathcal{Z}|k'\rangle\langle kk'|r_{12}^{-1}|mm'\rangle$$

$$\times[(\epsilon_m + \epsilon_{m'} - \epsilon_k - \epsilon_{k'})(\epsilon_m - \epsilon_k - \omega)]^{-1} + [(\epsilon_m + \epsilon_{m'} - \epsilon_k - \epsilon_{k'})(\epsilon_m - \epsilon_k + \omega)]^{-1}\ , \qquad (2.25)$$

$$\alpha_1^{d}(\omega) = \sum_{\substack{m,m'\\k,k'}} \langle m|\mathcal{Z}|k'\rangle\langle m'|\mathcal{Z}|k\rangle\langle kk'|(r_{12})^{-1}|mm'\rangle$$

$$\times[(\epsilon_m + \epsilon_{m'} - \epsilon_k - \epsilon_{k'})(\epsilon_m - \epsilon_{k'} - \omega)]^{-1} + [(\epsilon_m + \epsilon_{m'} - \epsilon_k - \epsilon_{k'})(\epsilon_m - \epsilon_{k'} + \omega)]^{-1}. \qquad (2.26)$$

The above expressions include the diagrams obtained by exchanging $\mathcal{Z}$ and $\mathcal{H}_2'(t)$ operators in diagrams (a), (b), (c), and (d). Some of the diagrams for $\alpha_2(\omega)$ which include two orders of $\mathcal{H}_1'$ vertices are shown in Fig. 5 and the corresponding expressions can be easily derived from the diagrams.

The comparison of $\alpha(\omega)$ with experiment is carried out by relating $\alpha(\omega)$ to the refractive index $n(\omega)$ at standard temperature and pressure by the relation

$$[n^2(\omega) - 1]/[n^2(\omega) + 2] = \tfrac{4}{3}\pi N_0 \alpha(\omega)\,, \qquad (2.27)$$

where N_0 is the number of atoms per cubic centimeter.[20] It must be noted that Eq. (2.27) applies strictly to noninteracting atoms and one has to take account of corrections due to interatomic interactions[4,21] in making accurate comparisons of theory and experiment.

The dynamic polarizability $\alpha(\omega)$ has poles on the

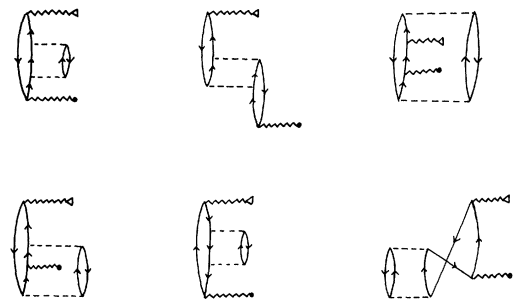

FIG. 5. Some higher-order diagrams contributing to $\alpha_2(\omega)$.

ω axis due to the energy denominators in the diagrams. The entire $\alpha(\omega)$ curve thus involves regions centered around the poles which resemble the anomalous dispersion effect in optical spectroscopy. While the values of $\alpha(\omega)$ in the neighborhood and beyond the first pole of ω are not very meaningful in view of our assumption of adiabatic response of the atom to the electromagnetic field, the poles of $\alpha(\omega)$ can nevertheless be interpreted as corresponding to the various excitation energies of the atom. The lowest-order approximation to these excitation energies is obtained from the denominator of $\alpha_0(\omega)$, namely,

$$\omega = \epsilon_k - \epsilon_m \quad . \tag{2.28}$$

This is the energy difference between one-electron states generated by the single-particle potential V_i that we have chosen. Thus, one obtains a measure of the extent of resemblance of V_i to the real physical potential by comparing the poles of $\alpha_0(\omega)$ with the experimental excitation energies. To introduce higher-order corrections to the poles of $\alpha(\omega)$ due to the consistency and correlation effects, it is necessary to sum the various classes of diagrams to infinite order. This can be carried out by a geometric series approximation which was found to be good in helium.[4,14]

III. RESULTS AND DISCUSSIONS

In this section, the results of the application of the method explained in Sec. II to the ground state of neon ($1s^2 2s^2 2p^6; {}^1S$) are presented.

We have chosen for our calculation the so-called V^{N-1} potential[4,6,13-18] for generating both bound and continuum single-particle states. The single-particle s states are generated by exciting the $2s$ electron to ks states, the radial equation being

$$\left(\frac{d^2}{dr^2} + \frac{20}{r} - 4\int_0^\infty P_{1s}{}^2 \frac{1}{r_>}\, dr' - 2\int_0^\infty P_{2s}{}^2 \frac{1}{r_>}\, dr' - 12\int_0^\infty P_{2p}{}^2 \frac{1}{r_>}\, dr' + 2\epsilon_{ks}\right) P_{ks}(r)$$

$$+ 2\int_0^\infty P_{1s} P_{ks} \frac{1}{r_>}\, dr'\, P_{1s}(r) + 2\int_0^\infty P_{2p} P_{ks} \frac{r_<}{r_>^2}\, dr'\, P_{2p}(r) = 0 \, . \tag{3.1}$$

The single-particle p states are generated by exciting the $2p$ electron to kp states. The corresponding radial equation is

$$\left(\frac{d^2}{dr^2} + \frac{20}{r} - \frac{2}{r^2} - 4\int_0^\infty P_{1s}{}^2 \frac{1}{r_>}\, dr' - 4\int_0^\infty P_{2s}{}^2 \frac{1}{r_>}\, dr' - 10\int_0^\infty P_{2p}{}^2 \frac{1}{r_>}\, dr' + \frac{4}{25}\int_0^\infty P_{2p}{}^2 \frac{r_<^2}{r_>^3}\, dr' + 2\epsilon_{kp}\right) P_{kp}(r)$$

$$+ \frac{2}{3}\int_0^\infty P_{1s} P_{kp} \frac{r_<}{r_>^2}\, dr'\, P_{1s}(r) + \frac{2}{3}\int_0^\infty P_{2s} P_{kp} \frac{r_<}{r_>^2}\, dr'\, P_{2s}(r) + \frac{16}{25}\int_0^\infty P_{2p} P_{kp} \frac{r_<^2}{r_>^3}\, dr'\, P_{2p}(r) = 0 \, . \tag{3.2}$$

The single-particle d states are obtained by exciting $2p$ electron to kd states. However, the V^{N-1} potential for this case is not unique and as in earlier work[15,16] we took an average of the potential over the six possible excited configurations using a single determinant in each case. The radial equation for d states is

$$\left(\frac{d^2}{dr^2} + \frac{20}{r} - \frac{6}{r^2} - 4\int_0^\infty P_{1s}{}^2 \frac{1}{r_>}\, dr' - 4\int_0^\infty P_{2s}{}^2 \frac{1}{r_>}\, dr' - 10\int_0^\infty P_{2p}{}^2 \frac{1}{r_>}\, dr' + \frac{4}{105}\int_0^\infty P_{2p}{}^2 \frac{r_<^2}{r_>^3}\, dr' + 2\epsilon_{kd}\right) P_{kd}(r)$$

$$+ \frac{2}{5}\int_0^\infty P_{1s} P_{kd} \frac{r_<^2}{r_>^3}\, dr' P_{1s}(r) + \frac{2}{5}\int_0^\infty P_{2s} P_{kd} \frac{r_<^2}{r_>^3}\, dr'\, P_{2s}(r) + \frac{16}{45}\int_0^\infty P_{2p} P_{kd} \frac{r_<}{r_>^2}\, dr'$$

$$\times P_{2p}(r)+\frac{96}{245}\int_0^\infty P_{2p}P_{kd}\frac{r_<^3}{r_>^4}\,dr'\,P_{2p}(r)=0\ . \quad (3.3)$$

We have used Clementi's[22] $1s$, $2s$, and $2p$ wave functions of neon in generating the potential in Eqs. (3.1)–(3.3). The $2s$ and $2p$ states obtained from Eqs. (3.1) and (3.2) should be identical to the Hartree-Fock $2s$ and $2p$ states, which may be used as a check on our numerical procedure. Our energy eigenvalues and wave functions for the $2s$ and $2p$ states in fact agree to the fourth significant figure with Clementi's results. As expected, the other hole state, namely, $1s$, has an energy -34.1270 a.u. which is lower than the Hartree-Fock energy -32.7728 a.u. due to the difference between the V^N-1 and the actual Hartree-Fock potential for the inner-hole states. This energy difference is corrected for by ladder diagrams.[5,6,13–18] The $1s$ wave function, however, was inappreciably different from Clementi's Hartree-Fock function and differences between the two were neglected in the evaluation of diagrams. In evaluating the diagrams, the continuum basis states have to cover the range $k=0$ to ∞. This entire range is effectively included by the use of Gauss-Laguerre quadrature technique,[23] which also reduces the computing time significantly. In summing over bound states, the ten lowest states for each angular momentum l were included explicitly and contributions from the rest ($n>10$) were included by the $n^{-3/2}$ approximation.[14–18,24]

We shall next consider our results for the polarizabilities and excitation energies. Before taking up the comparison of our end results with experiment, it is appropriate to list some of the features of the contributions from individual diagrams.

For purposes of discussion we shall divide the diagrams into three broad classes, – those that involve zero, one, and two orders, respectively, of $\mathcal{H}_1'$, contributing, respectively, $\alpha_0(\omega)$, $\alpha_1(\omega)$, and $\alpha_2(\omega)$ to the total polarizability $\alpha(\omega)$. The pertinent diagrams of these three classes are presented in Figs. 3–5. We shall first consider $\alpha_0(\omega)$ which arises from the diagrams in Fig. 3. Table I summarizes for four typical frequencies the contributions to $\alpha_0(\omega)$ from various modes of excitation. It is noted that $2p\rightarrow kd$ excitations make the largest contribution at low frequencies, followed by $2p\rightarrow ks$ which contributes about one-third of $2p\rightarrow kd$. The contribution from $2s\rightarrow kp$ is one order-of-magnitude smaller while $1s\rightarrow kp$ is negligible in effect. The relative importance of these various modes can, of course, be severely altered in the neighborhood of resonances, as for example at the highest frequency in Table I which is in the neighborhood of the $2p\rightarrow 3s$ transition frequency. It is of some interest to analyze the relative contributions from bound and continuum states. This information is presented in Tables II and III where the contributions from various bound excited states and continuum are listed for the $2p\rightarrow kd$ and $2p\rightarrow ks$ excitations. For the $2p\rightarrow kd$ excitations, the continuum excitations give almost 95% of the total for this mode while for the $2p\rightarrow ks$ excitations, the bound states contribute about 65% of the total. A similar behavior was also found for the $2p\rightarrow kd$ and $2p\rightarrow ks$ excitations in higher-order diagrams. These observed, preponderant influences of the continuum states on the major excitation process $2p\rightarrow kd$ suggest that in variational calculations the trial functions should incorporate directly or indirectly the features of the continuum states. The relative importance of continuum states contributions to the total $\alpha_0(\omega)$ is also illustrated in Fig. 6, where both the continuum contribution alone and the total (continuum and bound) are plotted. Except in the vicinity of singularities, the over-all continuum contribution is seen to represent about 80% of the total.

The diagrams in Fig. 4 which contribute to $\alpha_1(\omega)$ can be broken up into two subclasses, as described in Sec. II; namely, the consistency types in Figs. 4(a) and 4(b) and the correlation types in Figs. 4(c) and 4(d). Cancellation effects between direct and exchange diagrams 4(a) and 4(b), and 4(c) and 4(d), lead to the result that as far as interactions within the p shell are concerned, finite contributions arise only from consistency and correlation effects between electrons of opposite spin through diagrams 4(a) and 4(c). The cancellation effects between electrons of same spin are similar to the

TABLE I. Lowest-order contributions[a] $\alpha_0(\omega)$ to the total dipole polarizability $\alpha(\omega)$ of neon (^1S) from various excitations and various ω.[b]

Excitation[c]	$\omega=0.0$	$\omega=0.20$	$\omega=0.40$	$\omega=0.60$
$2p\rightarrow kd$	2.05787	2.11115	2.29813	2.76381
$2p\rightarrow ks$	0.61001	0.65475	0.85199	2.10719
$2s\rightarrow kp$	0.05076	0.05100	0.05177	0.05312
$1s\rightarrow kp$	0.00075	0.00075	0.00075	0.00075
Total	2.71939	2.81765	3.20264	4.92487

[a]All polarizabilities are expressed in a.u. To convert them into Å^3 (10^{-24} cm^3), multiply by 0.14818.

[b]Energies in a.u.

[c]k denotes both bound and continuum excited states.

TABLE II. Contributions to $\alpha_0(\omega)$ [a] for neon (^1S) from $2p \rightarrow kd$ excitations for various ω.[b]

Excitation	$\omega = 0.0$	$\omega = 0.20$	$\omega = 0.40$	$\omega = 0.60$
$2p \rightarrow 3d$	0.04295	0.04586	0.05753	0.09991
$2p \rightarrow 4d$	0.02226	0.02367	0.02923	0.04804
$2p \rightarrow 5d$	0.01220	0.01295	0.01588	0.02553
$2p \rightarrow 6d$	0.00727	0.00772	0.00974	0.01499
$2p \rightarrow 7d$	0.00466	0.00494	0.00603	0.00952
$2p \rightarrow 8d$	0.00314	0.00333	0.00405	0.00637
$2p \rightarrow 9d$	0.00222	0.00235	0.00287	0.00449
$2p \rightarrow 10d$	0.00222	0.00233	0.00284	0.00445
$\sum_{n=11}^{\infty} nd$ [c]	0.00903	0.00957	0.01120	0.01703
$2p \rightarrow$ continuum	1.95192	1.99843	2.15876	2.53348
Total	2.05787	2.11115	2.29813	2.76381

[a] All polarizabilities are expressed in a.u. To convert them into Å^3 (10^{-24} cm^3), multiply by 0.14818.

[b] Energies in a.u.

[c] Estimated by $n^{-3/2}$ rule. See Refs. 14 and 24.

result found for hyperfine interactions in atoms with p electrons in the valence shell.[15,16] Interactions between p and s electrons can, however, take place through all the diagrams in Fig. 4 since direct and exchange diagrams are different in magnitude and do not cancel. The diagrams involving p-p correlation and consistency effects are found to be one order-of-magnitude larger than the corresponding p-s diagrams. This result is not unexpected since there is stronger overlap between p orbitals than between p and s. As regards the relative importance of consistency and correlation effects, they make identical contributions at zero frequency, with the consistency effect increasing in relative importance at higher frequencies. The calculated values of $\alpha_1(\omega)$ at different frequencies ω are included in Table IV.

Some of the typical second-order correlation diagrams that we have investigated are shown in Fig. 5. In evaluating these diagrams, only $2p \rightarrow kd$ (both bound and continuum) excitations were included, in view of their dominating importance for $\alpha_0(\omega)$ and $\alpha_1(\omega)$. In contrast to the results in helium[4], the contributions from these higher-order diagrams for neon were found to be about two orders-of-magnitude smaller than $\alpha_1(\omega)$, and thus numerically insignificant. Thus the values of the total $\alpha(\omega)$ in Table IV are effectively the sum of $\alpha_0(\omega)$ and $\alpha_1(\omega)$.

In Fig. 7, our calculated refractive index func-

TABLE III. Contributions to $\alpha_0(\omega)$ [a] for neon (^1S) from $2p \rightarrow ks$ excitations for various ω.[b]

Excitation	$\omega = 0.0$	$\omega = 0.20$	$\omega = 0.40$	$\omega = 0.60$
$2p \rightarrow 3s$	0.34396	0.37716	0.53086	1.65326
$2p \rightarrow 4s$	0.04432	0.04742	0.06006	0.10832
$2p \rightarrow 5s$	0.01485	0.01490	0.01846	0.03100
$2p \rightarrow 6s$	0.00592	0.00628	0.00771	0.01275
$2p \rightarrow 7s$	0.00282	0.00299	0.00364	0.00607
$2p \rightarrow 8s$	0.00136	0.00143	0.00174	0.00300
$2p \rightarrow 9s$	0.00058	0.00060	0.00073	0.00138
$2p \rightarrow 10s$	0.00015	0.00015	0.00017	0.00050
$\sum_{n=11}^{\infty} ns$ [c]	0.00591	0.00720	0.00885	0.01200
$2p \rightarrow$ continuum	0.19014	0.19662	0.21977	0.27891
Total	0.61001	0.65475	0.85199	2.10719

[a] All polarizabilities are expressed in a.u. To convert them into Å^3 (10^{-24} cm^3), multiply by 0.14818.

[b] Energies in a.u.

[c] Estimated by $n^{-3/2}$ rule. See Refs. 14 and 24.

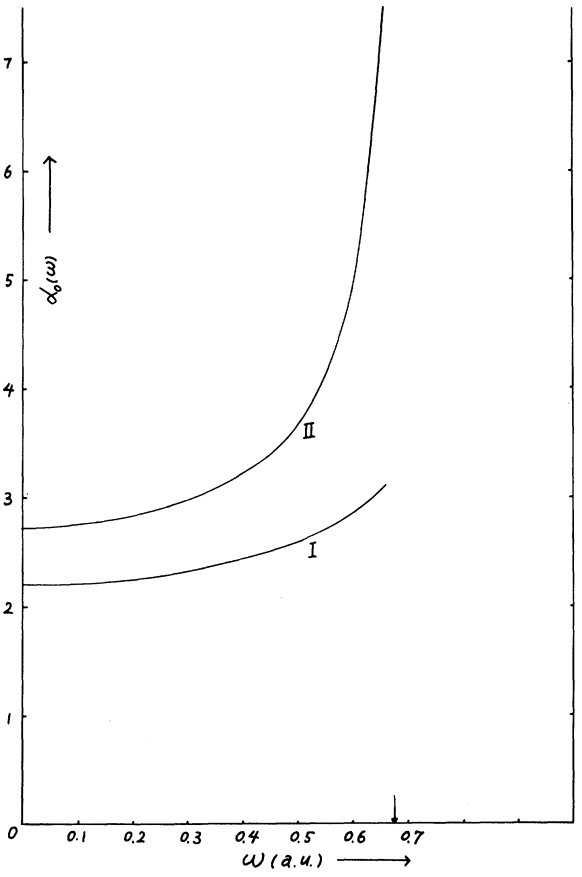

FIG. 6. Variation of the lowest-order contribution $\alpha_0(\omega)$ to polarizabilities of neon atom with angular frequency ω (in a.u.). Curve I shows the contribution from continuum states to $\alpha_0(\omega)$ corresponding to diagrams shown in Fig. 3. The arrow on the ω axis indicates the frequency correspondence to the first dipole excitation.

tion is compared with Cuthbertson and Cuthbertson's experimental results.[25] The one-electron results of Kaveeshwar, Chung, and Hurst[3] have also been included for comparison. While data on pressure dependence of $n(\omega)$ or the dielectric constant are not available for neon, Johnston, Oudemans, and Cole[21] point out that the pressure dependence appears to be much weaker than in helium and of the same sign. This behavior is not unexpected because of the anticipated cancellation of short-range and long-range interaction effects which predominate respectively in helium and argon. The excellent agreement between our calculated $n(\omega)$ and experiment reinforces our observation regarding the minor importance of consistency and correlation effects represented by $\alpha_1(\omega)$ and $\alpha_2(\omega)$. The magnitudes of consistency, first- and higher-order correlations symbolized by diagrams [Figs. 4(a)–4(d) and 5] for $\omega = 0$ are 2.4, 0.66, and 0.002%, respectively, relative to $\alpha_0(\omega)$. The comparable figures for helium are 6.46, 6.46, and 5.1, respectively. The nature of these results is to be expected physically, since helium has only one other electron which is more strongly affected by the perturbation of one of them while in neon the valence $n = 2$ orbitals contain eight electrons which are relatively less affected by what happens to one. This observation is similar to the Koopmans's theorem for excitation energies. In view of this minor importance of correlation effects on $\alpha(\omega)$, one-electron contributions calculated by other techniques should also agree well with experiment. The observed departure of about 10% between the results of Kaveeshwar, Chung, and Hurst,[3] and ours, can perhaps then be attributed to lack of flexibility of the variational function used by them.

The value of the static polarizability that we have calculated, namely, $\alpha(O) = 2.672$ a.u., compares very well with the value of 2.663 a.u. that is ob-

TABLE IV. Final results for the frequency-dependent polarizabilities $\alpha(\omega)$ of neon (^1S).[a]

ω[b]	$\alpha_0(\omega)$[c]	$\alpha_1(\omega)$[d]	$\alpha(\omega)$[e]	$10^8[n(\omega)-1]$[f]
0.0	2.71939	−0.04772	2.67167	6683.56
0.10	2.74291	−0.04812	2.69479	6741.41
0.20	2.81765	−0.04968	2.76797	6924.48
0.30	2.95847	−0.04977	2.90870	7276.54
0.40	3.20264	−0.05778	3.14486	7867.33
0.50	3.65999	−0.06721	3.59278	8987.86
0.60	4.92487	−0.10302	4.82185	12062.55
0.63	6.14852	−0.16088	5.98764	14978.96
0.66	11.83869	−0.82977	11.00892	27540.41

[a]All polarizabilities are in a.u. To convert them into Å^3 (10^{-24} cm^3), multiply by 0.14818.

[b]Energies in a.u.

[c]Contributions from diagrams shown in Fig. 3.

[d]Contributions from diagrams shown in Fig. 4.

[e]Total of column 2 and column 3.

[f]At STP, $N_0 = 0.26870 \times 10^{20}$ atoms/cm^3. See also Ref. 20.

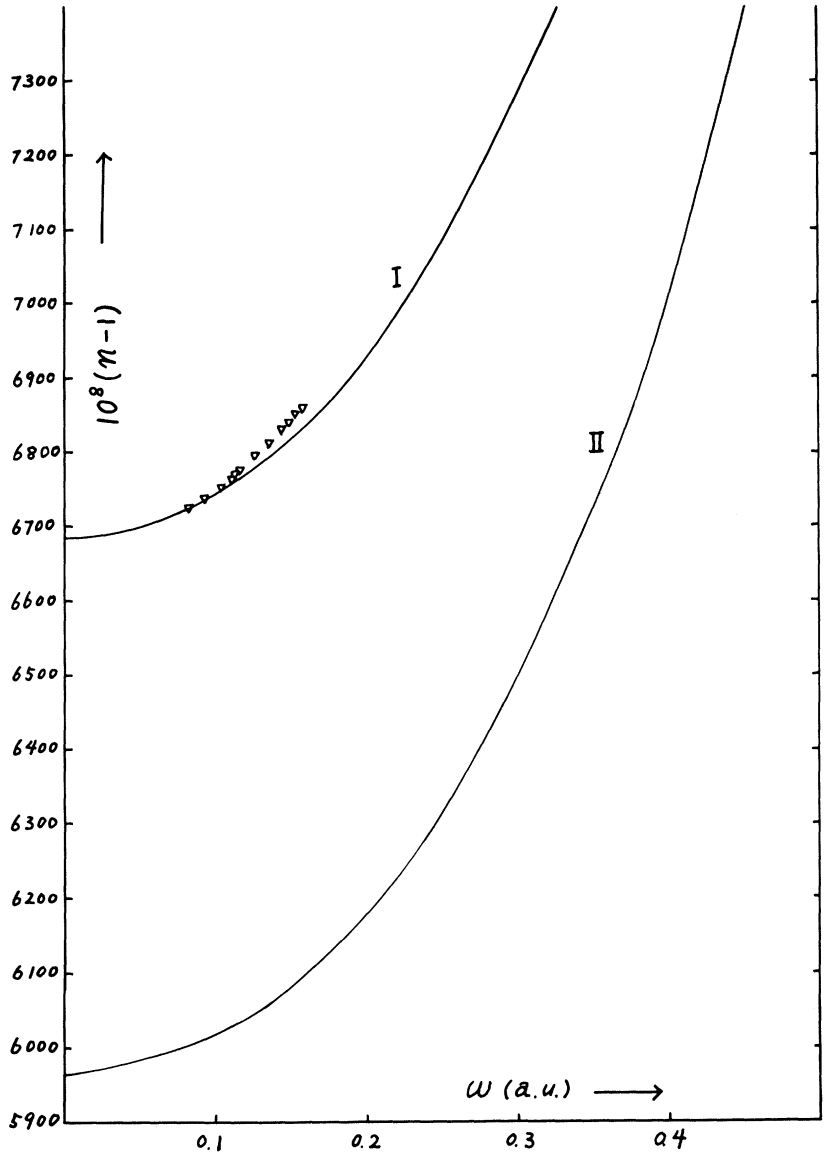

FIG. 7. Variation of $n(\omega)-1$ of neon, where $n(\omega)$ is the refractive index, with angular frequency ω (in a.u.). Curve I represents our final results including correlation effects, whereas Curve II gives the one-electron variational results of Kaveeshwar, Chung, and Hurst (Ref. 3). The "triangles" represent the experimental results of Cuthbertson and Cuthbertson (Ref. 25).

tained by extrapolating Cuthbertson's data to zero frequency.[26] Kaveeshwar, Chung, and Hurst's[3] value for $\alpha(0)$ was 2.382 a.u.

The singularities of $\alpha(\omega)$ are known to yield the excitation energies of the atom. In Table V, we list some of the $2p \rightarrow ns$ and $2p \rightarrow nd$ single-particle excitation energies together with the corresponding experimental data obtained from the table by Moore.[27] Since the excitations $2p \rightarrow nd$ can take place from any of the $m_l = 0, \pm 1$ states, and the hole in the $2p$ state for both $2p \rightarrow ns$ and $2p \rightarrow nd$ excitations can be in different j states, a number of closely spaced transitions are available for each value of n. Since we have neglected relativistic effects and have taken the average over configurations associated with $2p \rightarrow nd$ excitations, we cannot predict these splittings. Instead we have compared our excitation energies with one of the experimental transition frequencies for each n. The theoretical and experimental excitation energies listed in Table V are uniformly in agreement to within 7%.

IV. CONCLUSION

As in our earlier application to helium, the BG procedure has yielded, for neon, dynamic polarizabilities $\alpha(\omega)$ which produce excellent agreement with experimental refractive indices. The difference from helium is that the consistency and correlation effects play a less important role. A similar result is expected for the heavier rare gases. We would like to remark here that the BG proce-

TABLE V. Frequencies of spectral lines of neon (^1S).[a]

Calculated excitations		Experimental excitations[b]	
$2p \rightarrow 3s$	0.6744	$2p^5(^2P_{1/2})3s$	0.6192
$2p \rightarrow 4s$	0.7820	$2p^5(^2P_{1/2})4s$	0.7269
$2p \rightarrow 5s$	0.8141	$2p^5(^2P_{1/2})5s$	0.7594
$2p \rightarrow 6s$	0.8280	$2p^5(^2P_{1/2})6s$	0.7733
$2p \rightarrow 7s$	0.8352	$2p^5(^2P_{1/2})7s$	0.7806
$2p \rightarrow 8s$	0.8395	$2p^5(^2P_{1/2})8s$	0.7849
$2p \rightarrow 9s$	0.8422	$2p^5(^2P_{1/2})9s$	0.7876
$2p \rightarrow 10s$	0.8440	$2p^5(^2P_{1/2})10s$	0.7894
$2p \rightarrow 3d$	0.7947	$2p^5(^2P_{1/2})3d$	0.7401
$2p \rightarrow 4d$	0.8192	$2p^5(^2P_{1/2})4d$	0.7646
$2p \rightarrow 5d$	0.8304	$2p^5(^2P_{1/2})5d$	0.7759
$2p \rightarrow 6d$	0.8366	$2p^5(^2P_{1/2})6d$	0.7821
$2p \rightarrow 7d$	0.8402	$2p^5(^2P_{1/2})7d$	0.7858
$2p \rightarrow 8d$	0.8427	$2p^5(^2P_{1/2})8d$	0.7882
$2p \rightarrow 9d$	0.8443	$2p^5(^2P_{1/2})9d$	0.7898
$2p \rightarrow 10d$	0.8444	$2p^5(^2P_{1/2})10d$	0.7910

[a]Energies in a.u. (27.205 eV) calculated from diagrams in Fig. 3.
[b]Taken from Ref. 27.

dure for atomic problems has two main advantages. First, it allows a systematic study of many-body effects, and secondly, it allows a good quantitative treatment of one-electron effects in the presence of external perturbations through the use of a complete set of basis states. It is this latter feature of the method that is taken to most advantage in polarizability calculations. For the shielding factor[14, 17] of the nucleus in an external field, consistency and correlation effects would be of greater importance.

ACKNOWLEDGMENT

We gratefully acknowledge the computing time made available to us on the IBM 360-50 by the staff of the computing center at the University of California at Riverside.

†Supported by the National Science Foundation.
*Present address: Department of Physics, University of Utah, Salt Lake City, Utah 84112.

[1]M. Karplus and H. J. Kolker, J. Chem. Phys. 39, 1493 (1963); 39, 2997 (1963); 41, 880 (1964); 41, 3955 (1964).

[2]S. Sengupta and A. Mukherji, J. Chem. Phys. 47, 260 (1967).

[3]V. G. Kaveeshwar, K. T. Chung, and R. P. Hurst, Phys. Rev. 172, 35 (1968).

[4]N. C. Dutta, T. Ishihara, C. Matsubara, and T. P. Das, Phys. Rev. Letters 22, 8 (1969). A recent formulation [H. P. Kelly, Advan. Theoret. Phys., 2, 162 (1968)] for a time-dependent perturbation leading to Eq. (2.22) has been brought to our attention. See also N. C. Dutta, T. Ishihara, C. Matsubara, and T. P. Das, Bull. Am. Phys. Soc. 13, 1674 (1968).

[5]H. P. Kelly, Phys. Rev, 182, 84 (1968).

[6]N. C. Dutta, T. Ishihara, C. Matsubara, and T. P. Das, Int. J. Quant. Chem. 3, 32 (1969).

[7]A. Dalgarno, Advan. Chem. Phys. 12, 143 (1967).

[8]K. T. Tang, Phys. Rev. 177, 108 (1969).

[9]Robert O. Garrett, Shang Yi Ch'en, and Eng Choon Looi, Phys. Rev. 156, 48, (1967), and references therein; R. A. Brown and F. M. Pipkin, *ibid.* 174, 48 (1968); J. D. Lyons, Supriya Ray, and T. P. Das, *ibid.* 174, 104 (1968), and references therein.

[10]C. Matsubara, N. C. Dutta, and T. P. Das, Phys. Rev. (to be published).

[11]See Silvan S. Schweber, An Introduction to Quantum Field Theory (Harper and Row Publishers, Inc., New York, 1962), Chaps. 6 and 11.

[12]This normalization condition differs from the one we have adopted in earlier work (Refs. 15–18) where ψ was not normalized but instead $\langle\Psi|\Phi_0\rangle = 1$. In the latter case, we have to introduce the denominator $\langle\Psi|\Psi\rangle$ in Eq. (2.13) and after cancellation of unlinked terms in the numerator by the denominator the right-hand side of (2.15) follows.

[13]J. Goldstone, Proc. Roy. Soc. (London) A239, 267 (1957); K. A. Brueckner, Phys. Rev. 97, 1353 (1955); 100, 36 (1955); The Many-Body Problem (John Wiley & Sons, Inc., New York, 1959).

[14]H. P. Kelly, in Perturbation Theory and its Application in Quantum Mechanics, edited by C. H. Wilcox (John Wiley & Sons, Inc., New York, 1966), p. 215, and references therein.

[15]N. C. Dutta, C. Matsubara, R. T. Pu, and T. P. Das, Phys. Rev. Letters 21, 1139 (1968).

[16]N. C. Dutta, C. Matsubara, R. T. Pu, and T. P. Das, Phys. Rev. 177, 33 (1969).
[17]E. S. Chang, R. T. Pu, and T. P. Das, Phys. Rev. 174, 1 (1968); 174, 16 (1968).
[18]J. D. Lyons, R. T. Pu, and T. P. Das, Phys. Rev. 178, 103 (1969).
[19]T. S. Lee, N. C. Dutta, and T. P. Das, Phys. Rev. (to be published).
[20]All values for polarizabilities are quoted in a.u. In obtaining refractive indices from them we have used $N_0 = 0.26870 \times 10^{20}$ and the Bohr radius $a_0 = 5.29167 \times 10^{-9}$ cm. from Phys. Today 71, 48 (1964).
[21]D. A. Johnston, C. J. Oudemans, and R. H. Cole, J. Chem. Phys. 33, 1310 (1960).
[22]E. Clementi, IBM J. Res. Develop. 9, 2 (1965).
[23]Z. Kopal, Numerical Analysis (John Wiley & Sons, Inc., New York, 1961).
[24]H. A. Bethe and E. E. Salpeter, Quantum Mechanics of One- and Two-Electron Systems (Academic Press Inc., New York, 1957), p. 18.
[25]C. Cuthbertson and M. Cuthbertson, Proc. Roy. Soc. (London) A135, 40 (1932).
[26]A. Dalgarno and A. E. Kingston, Proc. Roy. Soc. (London) A259, 424 (1960).
[27]The experimental values of the transition frequencies are tabulated by Charlotte E. Moore, National Bureau of Standards Circular No. 467 (U. S. Government Printing Office, Washington, D.C., 1949), Vol. 1.

PHYSICAL REVIEW A VOLUME 1, NUMBER 3 MARCH 1970

Hyperfine Structure of the 2^3S_1 State of He^3†*

S. D. Rosner† and F. M. Pipkin
Lyman Laboratory, Harvard University, Cambridge, Massachusetts 02138
(Received 18 July 1969)

The zero-field hyperfine structure of the metastable 2^3S_1 state of He^3 has been measured by the optical pumping magnetic resonance method. The hyperfine transitions in a weak magnetic field were observed at low temperature in order to achieve narrow linewidths. Discussions of the theory of the hyperfine structure, the theory of the experiment, the apparatus, and the experimental procedure are presented. The final value for the hyperfine structure is 6 739 701 177 ± 16 Hz on the A-1 time scale. The fractional pressure shift of the hyperfine structure is $(-7.4 \pm 3.0) \times 10^{-9}$/Torr. The theoretical and experimental values for the hyperfine structure are compared, and the dependence on the nuclear structure is discussed.

INTRODUCTION

One of the important sources of information concerning nuclear and atomic structure is precision measurements of hyperfine structure intervals. The theoretical value for the hyperfine structure (hfs) depends upon knowledge of the atomic and nuclear wave functions, the electrodynamic corrections, and the values for the fundamental constants. One of the fundamental hyperfine intervals is that for He^3 in the metastable 2^3S_1 state. The hyperfine interval for this simple atomic state should be calculable to high precision; the agreement between the calculations and the measured interval can be used to test quantum electrodynamics and atomic-structure calculations.

This paper reports a redetermination of the hyperfine structure of the metastable 2^3S_1 state of He^3. The previous measurements of this hyperfine structure interval used an atomic-beam technique.[1,2] The precision of the measurements was limited by the transit time through the radio-frequency field; the linewidth was 40–55 kHz. The experiment reported here used an optical pumping technique to measure the hyperfine structure. The precision of the measurements was limited by exchange collisions between atoms in the metastable state and atoms in the ground state; the linewidth was 1–2 kHz. This large decrease in linewidth made it possible to reduce by more than an order of magnitude the error in the hyperfine structure interval.

The optical orientation of metastable He^3 was first reported by Colegrove, Schearer, and Walters.[3] They also showed that the cross section for exchange of metastability with the 1^1S_0 ground-state atoms was high enough to transfer the orientation to the ground state. This rapid metastability exchange process has the undesirable effect of severely broadening the magnetic resonance lines of the metastable state when the gas is at room temperature. It was predicted by Buckingham and Dalgarno[4,5] and demonstrated experimentally by Colegrove, Schearer, and Walters[6] that the metastability exchange cross section decreases rapidly as the temperature is decreased. The consequent narrowing of the metastable resonance lines has made possible a measurement of the hyperfine structure interval to a